ACS APPLIED MATERIALS & INTERFACES

www.acsami.org

Forum Article

3D Conducting Polymeric Membrane and Scaffold *Saccharomyces cerevisiae* Biofilms to Enhance Energy Conversion in Microbial Fuel Cells

Sajid Bashir,* William Houf, Jingbo L. Liu, and Shawn P. Mulvaney*

Cite This: https://doi.org/10.1021/acsami.1c20445

Read Online

ACCESS | Metrics & More | Article Recommendations | Supporting Information

ABSTRACT: Microbial fuel cells (MFCs) can spontaneously convert chemical energy into electricity using biocatalytic microorganisms and organic matter as fuel feedstocks. Three-dimensional cross-linked poly(vinyl alcohol)-based membranes were produced by a sol−gel method under homogeneous catalysis and used as the electrolyte to facilitate effective proton conduction. Under dry conditions, these polymeric membranes showed high water uptake (120%) and ionic conductivity (2.815 mS cm^{-1}). In the anode compartment, the scaffold *Saccharomyces cerevisiae* film biocatalysts were used to improve electron transfer to the cathode, using three major configurations to generate a higher power output. It was found that the graphene anchoring, red light (RL) stimulation, and methylene blue (MB) mediation-enhanced device performance. The electrochemically derived graphene improved the power and current density by 40% because of its high conductivity. The RL stimulation increased the power density by 80% because of a shortened electron flow path to complex III. The MB mediation also yielded a higher current density by 340% because MB can bypass the electron flow from complex II to cytochrome c and transfer electrons directly to complex III. The individual and collective increase in power output was due to more efficient electron flow from the electronic network permeating the biofilm. The generated electrons were transferred either to graphene as an energy-efficient direct transfer mode or to methylene blue as a long-range redox mediator for indirect transfer. Red light stimulation enhanced oxygen utilization efficiency and stimulated electrons in redox proteins enhancing electron flux. These processes generated higher power through the more efficient generation of electrons and faster transport to the external circuit. As society migrates from gasoline consumption to low carbon-based fuels, the MFCs become important in producing electrical energy with low net emissions.

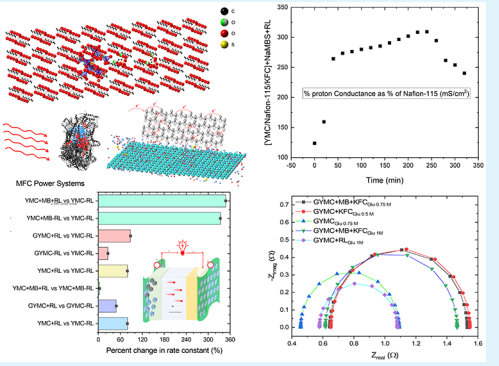

KEYWORDS: *microbial fuel cells, polymeric membrane, proton transport, biocatalyst, red light exposure, electrochemistry*

INTRODUCTION

The microbial fuel cells (MFCs) are electrochemical devices to convert chemical energy into electricity, using viable biocatalytic microbes without relying on abiotic catalysts and fossil fuels.[1] MFCs can mitigate environmental and ecological pollution[2] and eventually achieve carbon neutrality.[3] The electrochemically active microorganism can generate protons and electrons in the anodic compartment under aerobic or anaerobic conditions.[4] The electrons will be transferred through an external wire from anode to cathode,[5] whereas the protons diffuse via the electrolyte to complete the electrical circuits.[6] One example is to use sugar and acetate as a fuel source, where the electrochemical reactions occur (eqs 1a and 1b).[7] Those protons and other cations will migrate through a cation exchange membrane into the cathodic chamber.[8] If the diffused protons are to combine with the oxidant, normally oxygen (O_2), water (H_2O) will be formed by an oxygen reduction reaction (ORR).[9]

$$C_{12}H_{22}O_{11} + 13H_2O \rightarrow 12CO_2 + 48H^+ + 48e^- \quad (1a)$$

$$CH_3COO^- + 4H_2O \rightarrow 2HCO_3^- + 9H^+ + 8e^- \quad (1b)$$

The membranes have dual functions: a separator of cathode and anode compartments and an ionic conductor to allow cation diffusion.[10] The requirements for these membranes include high ionic conductivity, selective permeability, low internal resistance, and long-term stability.[11] The commonly used membranes based on sulfonated tetrafluoroethylene fluoropolymer-copolymer (Nafion) exhibit high proton conductivities (0.1 S cm^{-1}) while fully hydrated.[12] The membrane exhibits excellent thermal and mechanical stability and is extensively used as the electrolyte in proton exchange membranes.[13] However, these commercially available Nafion

Special Issue: Materials and Interfaces for Energy Storage and Conversion

Received: October 22, 2021
Accepted: December 10, 2021

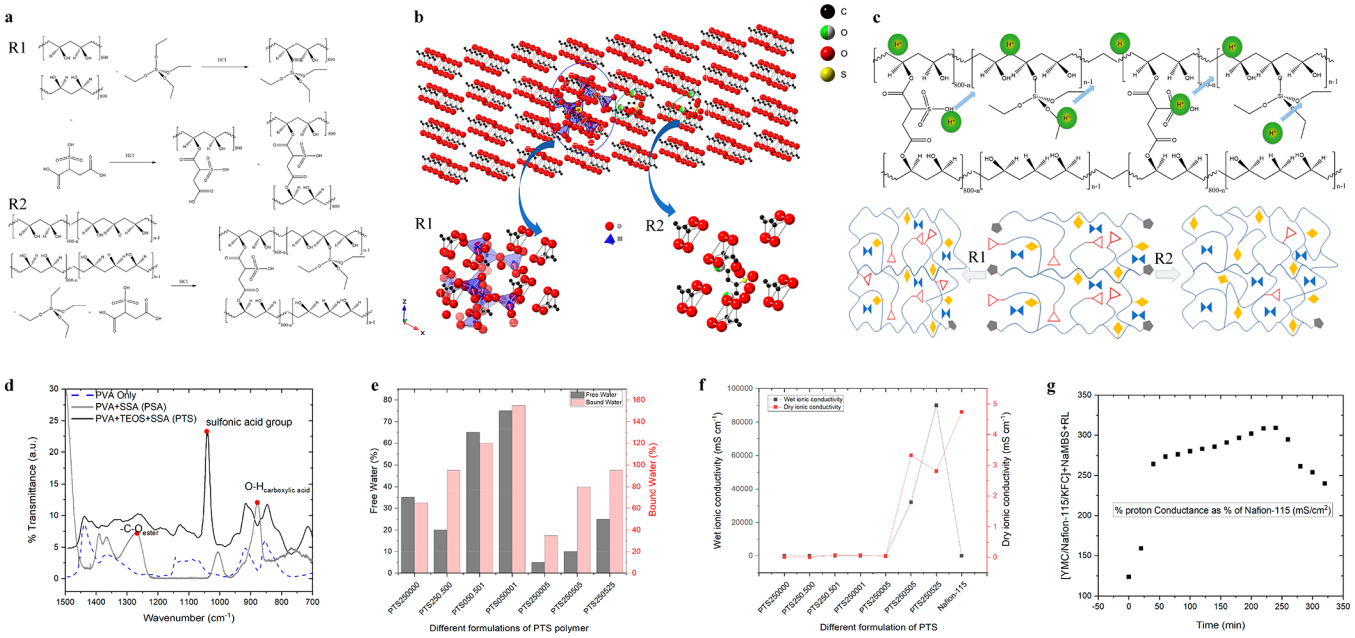

Figure 1. Design and characterization of a novel membrane (PTS) to enhance proton conduction. (a) Proposed reactions of dehydrolysis of TOES (R1) and esterification between PVA with SSA (R2). (b) Cross-linking effects between PVA & TOES (R1) and PVA & SSA (R2). (c) Proposed formation of a "proton wire" to facilitate H^+ diffusion through the PTS membrane with a tunable pore (R1) and charge (R2) densities. (d) FT-IR spectroscopic analysis of three representative specimens. (e) Water uptake of select PTS membranes. (f) Ionic conductivity of select PTS membranes under wet and dry conditions. (g) Ionic conductivity at the MFC device level.

membranes showed several drawbacks, such as high manufacturing expense, lacking selectivity, permitting leakage between anode and cathode compartments.[14] Therefore, a poly(vinyl alcohol) (PVA), the linear synthetic polymer, has been produced as an alternative electrolyte.[15] This family of membranes can be produced via partial or full hydrolysis of polyvinyl acetate.[16] The postmodification into a cross-linked macromolecule allows for tunable physical characteristics and chemical and mechanical properties.[17] Because of its high water solubility, PVA showed diverse applications in cartilage replacement,[18] desalination,[19] oxygen resistant films,[20] manufacturing adhesives,[21] and food preservation wrappings.[22] The possible hydrogen bonding between the alcohol functionality and bulk water can offer superior hydrophilicity to the Nafion membrane depending on PVA mass and the degree of hydrogen bonding.[23] The membrane has low proton conductance because of the absence of negative groups other than hydroxyl. Therefore, other carboxylic or sulfonic acid groups would increase proton conductance.[24] The introduction of sulfonic acid groups in the form of sulfosuccinic acid (SSA) increased proton conductance, where the negatively changed functionality can be cross-linked within the PVA membrane.[25] The interactions with generated silanol groups and the polycondensation of tetraethyl orthosilicate (TOES) can collectively enhance the mechanical stability.[26] However, the stiffness of these modified membranes (PTS) will result in cracking because of the incorporation of silica centers at a high mass percentage.[27] This research focused on optimization of synthesis variables to achieve the best performance of the functionalized membranes.[28]

The MFCs can operate as sealed power systems to maintain an anodic chamber under anaerobic conditions, allowing for the growth of obligatory exoelectrogenic microbes, such as brewer's yeast *Saccharomyces cerevisiae* (*S. cerevisiae*).[29] The microbes enable proton production and electron transfer by oxidizing carbon species, which can be from wastewater, biomass, and other feedstocks.[30] The electron flow will produce a direct electrical current, causing the potential differences between the anode and cathode compartments.[31] The aromatic sulfonation (in Nafion) of a membrane may result in acidity changes in the anode, causing microbe inhibitions.[32] The *S. cerevisiae* was used as a biocatalyst because of its resilience to environmental changes and its facile electron transfer mechanism.[33] Previously, it was shown that the *S. cerevisiae*, a eukaryote, was retrofitted into ethanol plants for in situ power generation;[34] in the short term, their configurations resulted in low device durability because of the poisoning of the biocatalyst.

Our approach aims to increase the robustness of the biocatalysts through enhanced proton transport. This enhancement can be accomplished using chemical or genetic modification of *S. cerevisiae* or fine-tuning of the redox respiratory proteins.[35] The red light (RL) was used to stimulate the electron transport within the respiratory complexes, for example, complex II. The binuclear copper iron monooxygenase can transmit RL as a form of "reducing power", thereby enhancing reactions summarized in eqs 1a and 1b. At the device level, advancement of exoelectrongenesis is expected to yield higher current and power densities, which was observed. In this study, the stimulation of yeast using 2.88 J cm^{-2} RL enabled the most efficient and effective electron transport, generating the optimal power output. In addition, the "reducing power" of RL mitigated the oxidative stress on *S. cerevisiae*, pronging the device's robustness.

The contribution of this study is three fold: (1) the synthesis of a novel cross-linked polymer membranes (PTS), showing high water uptake and ionic conductivity; (2) the improvement in energy density using biota-anchored films as an anodic catalyst; and (3) the application of RL to further enhance the robustness of the MFC devices. The specific morphologies of

https://doi.org/10.1021/acsami.1c20445
ACS Appl. Mater. Interfaces XXXX, XXX, XXX−XXX

the polymeric membrane were well-tuned using a one-step sol−gel method to form cross-linking structure. These membranes were found to conduct cations and protons from the anode to the cathode effectively through interpenetrative channels. The power characteristics of MFC devices were noticeably improved upon the using biota-anchored anodic catalysts through an indirect electron transfer mechanism. The RL exposure facilitated the *S. cerevisiae* metabolism to convert glucose into charge carriers and valuable carbon feedstocks.

RESULTS AND DISCUSSION

This paper will discuss the data in four sections: (1) the design and characterization of the novel membrane to enhance proton conduction, (2) the formation of biota-anchored anodic catalysts to increase the exoelectrogen rate, (3) RL stimulation to improve the device performance, and (4) the evaluation of the MFC performance to improve energy production.

Design and Characterization of a Novel Membrane. One-step sol−gel chemistry was used to produce 24 formulations of the cross-linked membrane with varying concentrations of poly(vinyl alcohol) (PVA), tetraethyl orthosilicate (TOES), and sulfosuccinic acid (SSA). The formula of the membrane was generalized as PTS. The optimized reaction conditions were found to control the reaction temperature at 95 °C for 2 h under magnetic agitation. The acidity (1.2−2.0) of the homogeneous catalytic cross-linking is critical to producing elastic and robust PTS. The amounts of PVA at 5−15 wt %, TOES at 2−5 wt %, and SSA at 5−35 wt % were controlled, respectively. The simplified reactions of the cross-linking procedure (Figure 1a, b) showed that the addition of TEOS initiated the cross-linking with PVA through the formation of intermolecular forces (Figures 1a, b-R1). At the same time, esterification between PVA and SSA occurs (Figure 1a, b-R2). The introduction of silica (SiO_2) can assist in the polar network with carboxylic and alcohol groups of poly(vinyl alcohol) and enhance thermal stability. The addition of sulfonic acid groups also caused an increase in ionic conductance when the negative functional groups were cross-linked within the PVA membranes. In this manner, the proton can be channeled (Figure 1c, upper panel) across the membrane network with tunable pore diameter, ionic charge, and heat tolerance by fine-tuning the mass weight percent of the three building blocks (Figure 1c, lower panel). The FT-IR spectrum (Figure 1d) at a wavenumber of 1240−1250 cm^{-1} is assigned to C−O ester groups, demonstrating the cross-linking reaction between the SSA and PVA chains. The spectral features of PTS at 3500−3200, 1040 and 750, and 920 cm^{-1} correspond to O−H within PVA, Si−OH, and Si−O−Si vibrations in TOES and −OH of the carboxylic acid functional group in SSA, respectively. Compared with the pure standard, the blue- or redshift illustrated the cross-linking among PVA/TOES/SSA components to produce crystalline PTS membrane. Both physical and chemical properties of the PTS membrane can be tuned via this cross-linking methodology because of the extension of a 3D network of the polyhydroxy structure of PVA when it was cross-linked with −OH groups.[36] The secondary attractions between polar groups (−OH) and residual silanol groups (H_4SiO-) can also enhance the mechanical stability.[37]

The pure PVA membrane is water-soluble (although it does not disintegrate) and shows flexibility within the water layer. Water uptake (Figure 1e) of the PTS membrane increases as the mass percent of SSA increases because of the formation of cross-linked pores able to trap water.[38] However, the increase in mass percent of TEOS resulted in a reduction of the water absorption because of the increased hydrophobicity of the membrane incorporating SiO_2 groups. The addition of TEOS appears to "stiffen" the membrane and loses its tendency to be dispersed within the water environment as a PTS film is no longer water-soluble.[39] The addition of SSA tends to reverse membrane inflexibility and brittleness, suggesting the membrane is slightly more water responsive. While the membrane is cross-linked, the linkages are not connected isotropically. The uneven cross-linkage creates pores, swelling, and fragility. The pores and hydrogen bonds can trap water into two distinct environments within the membrane. The presence of hydrogen bonds between the −OH of the PVA backbone and the cross-linked sulfonic acid group promotes bound water, whereas the pores near the outer surface promote occupancy of free water.[40] The latter can easily be discharged by heating the film at 120 °C, from which moisture and charcoaling effects were observed.[41] The difference in mass between the free and bound water suggests that the nature of the occupancy of the water can be altered through the addition of SSA.[42] Lesser SSA content promotes larger pores and occupancy of free water, whereas greater SSA would promote bound water and internal hydration within the membrane.

The ionic conductivity (Figure 1f) of the PTS membranes was evaluated under wet (fully hydrated gel precursor) and dry (epitaxially cast thin film) conditions. The results varied significantly from 0.38 and 0.0058 mS cm^{-1} for pure PVA polymer to 90003 and 2.815 mS cm^{-1} for PTS under wet and dry conditions. The microstructure in the PTS is consistent within the MFC device, where films with greater SSA incorporation yielded the greater dry conductance, although it was not proportional. At the device level, the membrane conductance increased after 50 min and was stable for 4 h and then decreased and was stable for 24 h (Figure 1g). The pseudovolcano relationship between the conductivity and TOES and SSA were obtained, indicating that the optimal mass percentages are 5 and 25 wt %, respectively. With the TOES increase, the ionic conductivity increased slightly but steadily when the plateau reached 10 mass%. This phenomenon resulted from the presence of SiO_2 with higher hydrophobicity, lower water content, and lower charge distribution. The SSA showed a stronger impact on the PTS conductivity than TOES. This nonlinear trend of ionic conductivity was also obtained because of the proton donor and carrier sulfonic acid group ($-SO_3...-H^+$), which occupy pores within the polymer network through the entrapment of water molecules.[43] The pore formation and gelation continue after sol-suspension synthesis and during the film casting process, which is sensitive to temperature and humidity variations.[44]

In general, the presence of negatively charged groups will increase the ion exchange and the conductance. The charge carriers are structured within the polymer pores, retaining bound water molecules. Therefore, a polymer with fewer negative groups may exhibit greater intrinsic proton conductivity than those with greater negatively charged groups inaccessible to bound water.[45] The water occupancy enhances the Coulombic charge distribution because of the hydrogen bonds between the carboxylic acid side group, the sulfonic groups, and the bound water.[46] A postfunctionalization of the PTS membrane using sodium ion exchange enhanced the MFC performance (Figure 4d). The advantage of this

https://doi.org/10.1021/acsami.1c20445
ACS Appl. Mater. Interfaces XXXX, XXX, XXX−XXX

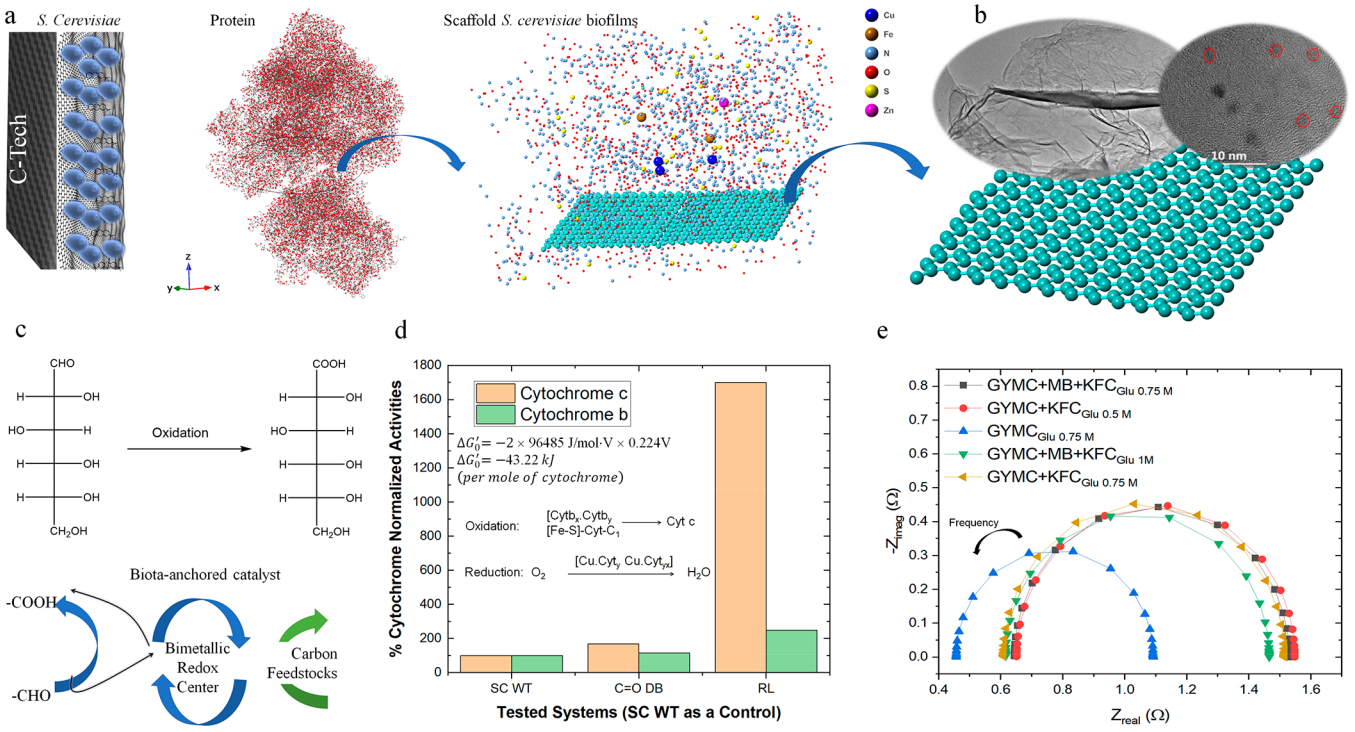

Figure 2. Design and evaluation of biota-anchored anode film catalysts to facilitate glucose oxidation. (a) Synthesis flowchart of the anode catalyst. (b) Transmission electron microscopic image of GQDs (1.85 ± 0.22 nm). (c) Oxidation of glucose to gluconic acid as one possible reaction using the biota anchored catalyst. (d) Thermodynamically favored reaction of cytochrome activity with glucose as feedstock. (e) Electrochemical impedance spectroscopic Nyquist plot for MFC devices with different configurations.

approach was that a lower mass weight percent of sulfosuccinic acid was used to fabricate membranes with the same required conductance. These PTS membranes were more flexible, easier to manipulate, less acidic relative to Nafion, and less hazardous to the biofilms.

Formation of Biota-Anchored Anodic Catalysts. The power output and long-term stability of the MFC power system were affected by the strain of yeast, its growth rate, the substrate affinity, the kinetic and biomass transfer, and the thermodynamics of the anodic reaction. The choice of the organism in a fuel cell is an important component to generate power output, related to the availability of organic feedstock and oxygen.[47] Yeast is a unicellular eukaryote that can grow aerobically and convert sugars to carbon dioxide and water or anaerobically to alcohol, gluconic acids, or glucose-lactones. Yeast also has significant gene homology with human respiratory proteins, especially with cytochrome c oxidase, which accepts electrons and converts molecular oxygen to water using excess protons and chemical energy.[48]

The biota-anchored catalytic films were prepared by enabling an attachment between select exoelectrogenic *Saccharomyces cerevisiae*.[49] This strain of microbes was chosen because of the ease of culture and capacity to transfer electrons extracellular RL or perform respiration at the anode. Two commercially available substrates (C-Tech and Avcarb) were used to form biofilm catalysts. The graphene quantum dots (GQDs) were prepared using a combined electrochemical exfoliation and ultrasonication approach to ensure high purity and electronic conductivity. The anodic catalyst was composed of triple components (Figure 2a) with enhanced substrate affinity to the GDQs and *S. cerevisiae* via an active hydrophobic attraction. Upon nanomodification, these biofilm anodes rapidly respond to the external environmental changes and self-regulate their structures.[50] Our observations suggested that direct biofilm growth occurred because of the self-assembly effect via controlling the attraction between microbes and hydrophobic GQD surfaces. These hydrophobic GQDs (Figure 2b) with high purity and conductivity showed dual functions, acting as reactive sites for *S. cerevisiae* for proton formation and "conducting wires" for electron transfer. This intrinsic hydrophobic GQD serves as a soft template to attract microbes by controlling the emulsion surface charging. The resultant anodic biofilm catalysts displayed high conductivity due to the extension of electron transfer by a conductive microorganism. The current at the device level characterized indicated that the yeast was aligned with the GQD distribution.

The biocompatible and robust anode catalysts demonstrated large open cavities and active sites for glucose to be oxidized to gluconic acid and protons (Figure 2c). The biocompatibility was examined using the direct device voltage and the optical density (OD) of *S. cerevisiae* after 24−48 h of exposure. The results confirmed that the bulk resistance of the GQD-biota was lower than that of Avcarb and our uncoated membrane or with the Nafion membrane. The direct voltage for the control was 1.21 V, for GQDs was 1.11 V, and for Nafion was 1.12 V, respectively. These measurements indicated GQD anchoring facilitated external electron transport, enabling improved current densities at the device level. The optical density measurements after 48 h of exposure of yeast on the membrane indicated that growth was sensitive to the catalytic support surfaces. The estimated OD values suggested that GQDs yielded the highest growth rate (0.42 au), whereas Nafion had the lowest (0.12 au) growth compared to a control value of 0.40 au. This observation confirms our hypothesis that the inclusion of GQDs will enable templating of the anchored biota without compromising cellular growth. The energy for

https://doi.org/10.1021/acsami.1c20445
ACS Appl. Mater. Interfaces XXXX, XXX, XXX−XXX

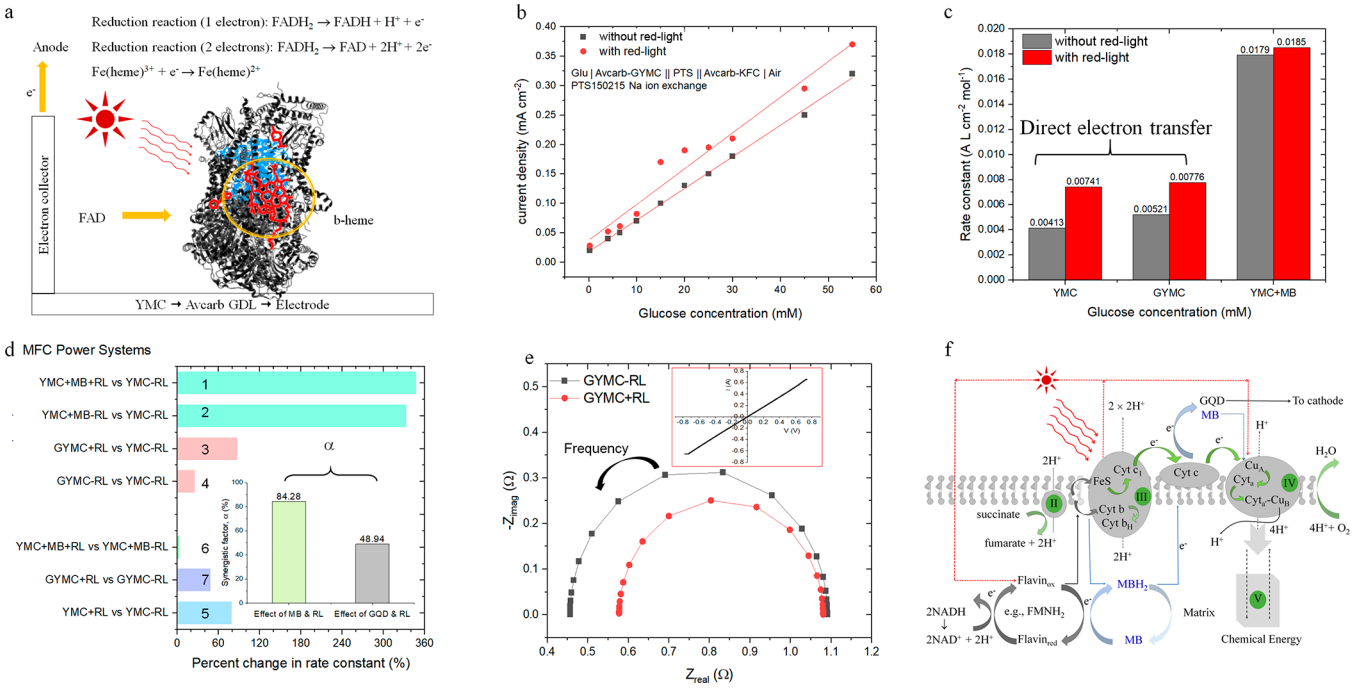

Figure 3. Red light enhancement of the MFC power system. (a) Proposed redox reactions are stimulated by RL, resulting in increased current and power densities. (b) Change of current density as a function of glucose in the absence and presence of red light. (c) Rate constant for representative MFC systems composed of yeast (YMC), graphene (GYMC), and yeast with methylene blue as electron meditator (YMC+MB). (d) Percent change in the rate constant of different systems, including the synergistic factor increase as the inset. (e) EIS and CV (insert) of the MFC device under RL stimulation compared with unexposed systems in the presence of glucose (1 M). (f) Proposed mechanism for both MB and RL influence on cytochromes related to the observed increase in current and power densities.

cellular growth is derived from environmental carbon, such as glucose or other organic matter. When glucose is used as the carbon source, it can be oxidized to gluconic acid and a proton by a two-electron oxidation process (Figure 2c). Other possible oxidations will generate ethanol under low oxygen availability, whereas CO_2 will be produced under high oxygen conditions. The oxidation of glucose to various intermediates is favored thermodynamically because of the high reduction potential of the cytochromes in the respiratory system of *S. cerevisiae*. The actual magnitude of the driving force is related to the availability of oxygen and the type of carbon source.

The MFC power systems were evaluated spectroscopically to derive the cytochrome activities of *S. cerevisiae* (SC) wild type (WET) under two conditions, glucose addition and RL stimulation. The SC WET grown in low glucose media exhibited relatively low cytochrome activity because of the limited availability of charge carriers (H^+ and e^-). Upon addition of a higher concentration of glucose, or exposure to the RL with a radiant energy of 2.88 J cm^{-2}, a concomitant increase in cytochrome activity was observed, indicating a high charge flux. The normalized plots (Figure 2d) showed that cytochrome b is subject to minor changes upon adding glucose and under RL stimulation or no stimulation compared with SC WET. On the other hand, cytochrome c undergoes significant changes, especially under RL from 100 to 1700% (equivalent to a synergistic increase of 94%), indicating that cytochrome c is the major factor to determine the redox reaction from cytochrome c to the terminal electron acceptor.

The spontaneity of the oxidation reaction in the anode compartment was driven using the change in Gibbs free energy, $\Delta G_0' = nF\Delta E_0'$. This $\Delta G_0'$ is determined between the net, reducing the potential between several coexisting cytochromes in oxidized and reduced forms. For example, cytochrome c can be reduced by the cytochrome bc1 complex. Alternatively, the reduction can be achieved using redox mediators, such as soluble flavin or binuclear copper iron−sulfur proteins. The difference between the potentials of cytochrome c and b is +0.254 − (+0.030) = +0.224 V. Therefore, the Gibbs energy change can be calculated by $\Delta G_0' = -2(96.485\ \text{J/V} \times 0.224\ \text{V}) = -43.22$ kJ (per mole of each cytochrome), confirming the spontaneous reaction.[51] This is an upper value as the redox potential for the various cytochromes of yeast is slightly lower than their mammalian counterparts but supports a spontaneous reaction, especially after RL stimulation.

The electrochemical performance of MFC devices with different configurations was systematically evaluated using electrochemical impedance spectroscopy (EIS) under ambient conditions. The key components investigated were yeast-methyl cellulose (YMC), GQD-supported catalyst (GYMC), and the addition of either methylene blue (MB) or potassium ferrocyanide (KFC). The fitted EIS data (Figure 2e) indicated the charge transfer resistance (R_{ct}) ranged from 0.7 to 1.0 Ω, indicating the biota-anchored catalysts showed high reactivity because of the large porosity and small particle size of GQD-based support. The synergistic factor of the multicomponent device was estimated using the R_{ct} of a representative device 1 (GYMC+MB+KFC), device 2 (GYMC+KFC), and device 3 (GYMC+MB). The calculated data of device 1 showed an overall increase of 56.85%, suggesting that the combination of devices 2 and 3 provide greater enhancement than either pristine system. In the absence of charge carriers such as MB or KFC, the R_{ct} of the base YMC device was the highest, confirming that the electron transfer mechanism for yeast was

https://doi.org/10.1021/acsami.1c20445
ACS Appl. Mater. Interfaces XXXX, XXX, XXX−XXX

mediated. The EIS plot also confirmed that the utilization of GQDs gave the fastest electron transfer kinetics.

To further investigate this concept, we applied carbon-black-supported platinum nanoparticles (Pt NPs) as the catalyst at the cathode and both compartments. The R_{ct} of the MFC systems with Pt as the cathodic catalyst ranged from 119 to 175 Ω because of the improved kinetics of the oxygen reduction reaction (ORR). As anticipated, the addition of Pt into the anodic compartment resulted in sluggish reactivities of the microorganism, as evidenced by a one-fold increase in the R_{ct}. This observation confirmed that the MFC could operate noble metal independently, further lowering manufacturing costs. In summary, the triple components enable an amphiphilic postmodification, where both protic and aprotic channels are accessible for glucose adsorption under ambient conditions. The yeast via engineered biota-on-surface nanomaterials provides a viable platform to improve electron transfer through a spontaneous biochemical reaction. As anticipated, biota-anchored biofilms improve the MFC devices' electrochemical performance compared to MFCs composed of Nafion-based electrolytes.

Red Light Stimulation to Improve Device Performance. The RL was selected on the hypothesis that it would excite electrons from the 2p to 3d orbital of transition metal ions found in cytochrome heme and flavins. The wavelength corresponding to this transition was calculated to be 653 nm using the Rydberg equation. The wavelength used in our device was 635 nm, sufficient to elicit these transitions. Furthermore, it was speculated that RL stimulation would promote electron transfer to a mobile flavin from complex II (succinate dehydrogenase)/III (cytochrome bc_1 complex) to complex IV (cytochrome c oxidase), which is central to switching from fermentation to respiration.[52] The yeast used in the MFC showed a high power output due to its gene homology with human respiratory proteins, especially with cytochrome c oxidase. This cytochrome accepts electrons and converts molecular oxygen to water using excess protons and chemical energy. The electron flow mechanism would involve cytochrome c gaining an electron from a flavin as electron donors, such as a flavin adenine dinucleotide (FAD, Figure 3a). The redox reactions of the flavin were listed in the inset of Figure 3a.[53]

By promoting electron transfer to the cytochrome heme, the current density at the device level is expected to increase, which was observed (Figure 3b). Glucose feedstock is converted to chemical energy in an MFC, increasing current density with increased concentration. Comparing the current densities across varying glucose concentrations suggested the reaction order is pseudo-first-order. An in-depth examination indicated that the kinetics of the reaction increased by 14−42% after RL exposure under lower concentrations than 10 mM, whereas the rate increased by 16−70% at concentrations higher than 20 mM. The data suggest that mass diffusion as a limiting step is unlikely at lower feedstock concentration but might become more prominent at higher concentrations.[54]

Although the generated protons migrate through the PTS membrane to the cathode compartment, the flow of electrons can take two possible paths. One possible path is through an electron mediator such as methylene blue (MB), which would receive the electron from a soluble flavin and transfer it to cytochrome c oxidase. Alternatively, the yeast methylcellulose (YMC) biofilm could facilitate direct electron transport near the electrode surface (Figure 3c). Conjugated π-systems facilitated electron transfer when proximate to flavins and GQDs, especially under a red light. The plot of the rate constant using three MFC device configurations confirms the hypothesis that the current density is higher under RL exposure for the YMC configuration. When GQDs were used, the rate constant was even greater, confirming that direct electron transport from GQDs to the current collector occurred. When an electron mediator in MB was used, the current density was the highest. The relative increase in current density to RL exposure was 79% for the YMC device, 49% for GYMC, and 3.4% for MB compared to the unexposed devices.

The increase in current density between YMC and YMC +RL devices is due to the ability of RL to stimulate electron flow from complex II → flavins → cytochrome c → complex III and ultimately to complex IV. Therefore, RL-assisted electron flow to the flavins can explain the observed increase in current. For the GYMC device, two factors contribute to the observed current increase. The first factor is the inherent conductance of GQDs as an electron path with lower resistance to the external circuit. The second is a lower energy pathway from complex II → flavin → GQDs, instead of flavin → cytochrome c → complex III if the flavins and GQDs are close to the yeast membrane. In the YMC+MB device, the greatest current density indicates that electron mediators from within the cell facilitate electron transfer.[55] The feedstock would act as an electron donor, GQDs as the conduit, and the electrode as an acceptor.[56] The kinetic plot indicates that direct and indirect factors occur, resulting in a synergistic increase. In-depth analysis between the three representative devices indicates that 9% of the total increase was by direct electron transport (GYMC). The remaining 91% increase in current density is due to the MB mediation, supporting the contention that electron transport in yeast is largely due to the mediated mechanism. In this indirect transfer, flavins pass electrons to the mediators, which transmit them to the terminal electron acceptor, complex IV.

The power and current curves of 33 different MFC devices were evaluated, and data for three select systems are summarized in Figure 3d. The percent change of the rate constant for these systems was calculated using YMC as the reference configuration with three variables. The RL stimulation, GQD (G) scaffold, and MB mediation were found to play critical roles in influencing device performance (Figure 3d, 1 and 2). The synergistic factors as shown in the inset were estimated using the equation $\alpha = (k_{ab}/k_a + k_b)100\%$. The comparison of the plots showed that RL irradiation of 2.88 J cm^{-2} increased the rate constant by approximately 80% (Figure 3d, 5 and 7). The GQD utilization in YMC showed about a 35% increase due to the π-electron transfer (Figure 3d, 4). The MB showed the highest impact on the current density increase of the YMC systems (300%, Figure 3d, 2) due to more facile kinetics than an increase in ion flux. The increase in current due to the combined effect from RL and G was about 100% (Figure 3d, 3). When the YMC system was evaluated under collective MB and RL conditions, a modest increase of 5% was obtained (Figure 3d, 6), suggesting that the MB and RL operate under the same molecular circuitry. The electron transfer to the flavins is stimulated by RL between complex II → complex III (cytochrome bc_1 complex) → complex IV (cytochrome c oxidase supracomplex), increasing electron flow.[57] A similar increase is observed when MB is used, suggesting that MB intercepts the electrons and passes them directly to complex III. When both are used, the increase in

https://doi.org/10.1021/acsami.1c20445
ACS Appl. Mater. Interfaces XXXX, XXX, XXX−XXX

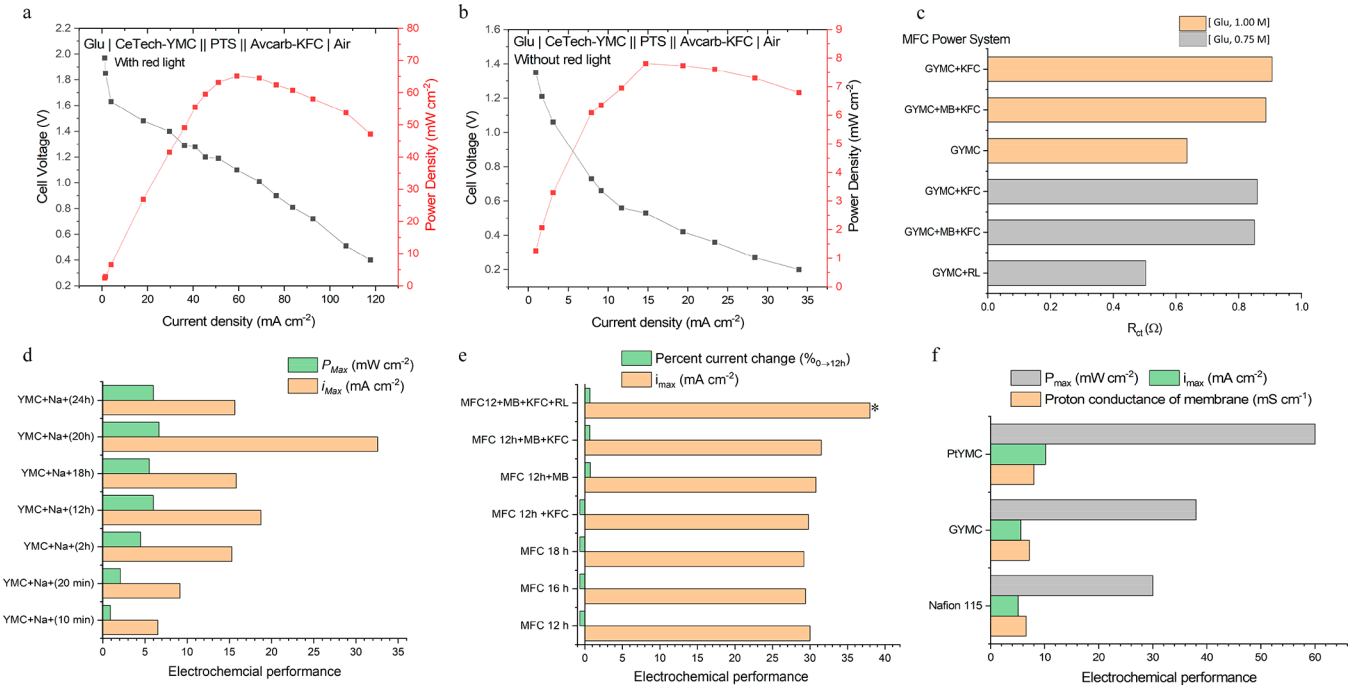

Figure 4. Evaluation of MFC energy production. (a) $I-V$ curve of a select MFC configuration under RL stimulation (scaled by $100/\pi$ ("tri contatri-") which converts to m^2 by ×10 (120 scaled cm^{-2} → 1200 mA m^2 or 650 mW m^{-2}). (b) Low power configuration without RL stimulation (scaled cm^{-2}) converts to m^2 by ×10). (c) Charge transfer resistance of select MFC power systems. (d) Maximum power and current densities associated with Na^+ ion exchange duration. (e) Stability of MFC power systems with different configurations. (f) Electrochemical evaluation of MFC systems with different catalysts.

electron flow is modest because RL or MB alone has already achieved the maximum rate.

Our study showed the MB influence on the device performance the most, followed by RL and GQDs. The MB was used as a two-electron mediator with a standard reduction potential of +0.01 V at pH 7.[58] Previously, MB was also an effective mediator with the highest power density compared to a series of electron mediators in a yeast fuel cell.[59] The RL intensity was optimized to be 2.88 J cm^{-2}, corresponding to a 60 min exposure based on different exposure times of 15−120 min. Although the current density increased at higher irradiation durations, the greatest single percent gain relative to 15 min of exposure was 60 min. The Nyquist curve of GYMC in the presence of RL at 2.88 J cm^{-2} flux (Figure 3e) confirmed that charge transfer resistance was less (R_{ct} = 0.51 Ω) than in the unexposed device (R_{ct} = 0.64 Ω). This was also seen in the cyclic voltammogram, which showed negligible hysteresis (insert of the figure). In summary, the two dominant factors that led to the greatest increases in current densities were 1 ppm MB or 2.88 J cm^{-2} red light. To further delineate this biocircuitry, we reviewed the application of MB in yeast or mammalian systems.

Lee et al. used yeast-derived complexes reconstituted into nanoscale model membranes,[60] demonstrating that in the presence of succinate as the carbon source and complex II inhibitor NAPQI, the MB (<3 μM) reduction (to MBH_2) occurred, at the usual rate. However, succinate oxidation in the absence of MB was retarded.[61] These two observations link MB and succinate oxidation and point to the source of electrons as complex II as an acceptor and succinate as a donor. The same study also found that upon adding oxidized cytochrome c, MBH_2 was readily oxidized back to MB. These two separate observations indicate that MB in mammals can bypass complex I (NADH: ubiquinone oxidoreductase) and complex II and pass electrons from succinate or glucose to cytochrome c. Complex III can restore the energy balance when inhibition occurs upon receiving electrons.[62] Our observations are consistent with the above study that electron flux increases in yeast with no inhibition (Figure 3b−e and insets).

Collectively, these observations demonstrate that endogenous flavins pass electrons to the MBH_2 from inside the cell and MB to the electrode directly.[63] The oxidized mediators that pass through the cell membrane are reduced, reach the electrode, transfer the electron, and undergo oxidation to complete the redox cycle. In the yeast, the electron transfer would be between the flavin and the cytochrome c oxidase heme group, where Fe(III) can act as an electron acceptor.[64] Lin et al. demonstrated that MB increased oxygen consumption and glucose uptake in HT22 cells,[65] also confirmed in a second study even when the respiratory proteins were inhibited.[66] It was suggested that MB could cycle between the oxidized form (MB) and reduced form (MBH_2), which in turn is oxidized by cytochrome c. The cytochrome c passed electrons to cytochrome c oxidase and then terminal electron acceptor by passing the electrons to oxygen. In the absence of oxygen, iron(III) from the heme or redox-active coppers can act as electron acceptors (Figure 3f). These redox-active proteins also have other metal cofactors such as Ca^{2+} and Zn^{2+}, which are known to be sensitive to visible light.[67] Our observations suggest the RL or MB can also act upon the same flavin-cytochrome c heme system.

Phenomenologically, stimulation of RL may increase electron flux through electron acceptor cytochromes. Red light may also assist in increased utilization of available oxygen, known as oxygen capacity. The increased oxygen capacity

https://doi.org/10.1021/acsami.1c20445
ACS Appl. Mater. Interfaces XXXX, XXX, XXX−XXX

would lead to increased energy production without increasing the rate of electron flux. Our observation of increased current density after RL stimulation or MB mediation supports the hypothesis of increased electron transport within the cytochromes. Lin's study[66] also yields a second plausible hypothesis to explain the higher current densities. They were able to show that in their system, the higher current from MB was due to increased oxygen utilization rather than electron flux. If yeast cells utilize residual oxygen, glucose can be metabolized more efficiently, resulting in increased proton generation and bioenergy. At the device level, an increased current is expected when a fuel cell is operating with oxygen instead of air, like the increase in current density due to more efficient oxygen utilization, which we observed.

Evaluation of MFC Performance. A two-chamber MFC power system with different configurations has been constructed using the above anode and PTS polymeric membrane to investigate device behavior. The graphite-supported Pt was used in the cathode compartment to improve the oxygen reduction reaction compared with no-catalyst devices. The MFC configurations and feedstock concentrations were varied under the same measurement conditions. The impact of GQDs, RL, and MB on power output was also investigated. The MFC system with a configuration of CTech|YMC||PTS100220|KFC|Avcarb showed high maximum power and current densities (65 scaled mW cm^{-2} and 120 scaled mA cm^{-2}, Figure 4a) upon RL stimulation, whereas without RL exposure, lower performance was obtained (8 scaled mW cm^{-2} and 35 scaled mA cm^{-2}, Figure 4b). The change in glucose concentration in the absence and presence of RL can provide information on current density as an indicator of the redox kinetics in the MFC anode and cathode chambers. From the plots of power curves (Figure 4a, b), the devices under RL showed a faster rise and decline than the unexposed ones. This suggests that mass transfer of glucose is not a limiting step because of its more efficient metabolism under RL. A glucose concentration less than 100 mM, RL exposure, MB mediation, and GQD anchoring collectively resulted in a lower charge transfer resistance (Figure 4c). The approximation of a third-order polynomial plot based on various glucose concentrations suggested that different factors collectively contribute to the overall kinetics. The factors are mainly glucose and oxygen diffusion to the electrode and the resistance of the biofilm to the generated electrons.

To enhance the device's robustness, we carried out postfunctionalization of the PTS membrane using Na^+ exchange. The maximum current and power for various ion exchange durations of MFC devices were evaluated. It was found that 20 h of Na^+ exchange yielded the greatest percent increase in power with a bimodal distribution for current density (Figure 4d). The data suggested that all exposed sites were fully exchanged by 20 h and that charge repulsion may retard ion mobility for prolonged durations. The device stability study indicated that the current change after 12−18 h was less than 1%, compared to after a 10 min operation. The maximum power followed the previous trends that MFC devices without mediators yielded the lowest values. Furthermore, the use of red light, graphene, and MB at the anode or KFC at the cathode resulted in the greatest power output (Figure 4e*), accordingly.

The GQDs resulted in higher power densities by 40% (GYMC vs. YMC), confirming that these electrodes are good electron acceptors and conductors through their unhybridized p_z orbitals. The reduction potential is positive relative to the mediators or glucose from the extracellular matrix, allowing acceptance and transport of electrons to generate power. The yeast allows for formations of interactive nanomaterials by a simplified feasible wet chemistry, securing a homogeneous tunability of structure and properties from the molecular or atomic level (Figure 2a, b). The effect of anode and cathode modification on improving device efficiency was investigated using GQDs at the anode and platinum at the cathode (Figure 4f). The high-power densities of GQDs are due to their high surface area, ability to transmit electrons along its surface, and conductivity and that of platinum is due to the inherently fast kinetics of its oxygen reduction reaction.

The relationship between the current density of the devices and oxygen accessibility to the microbes was indirectly obtained from voltage−current curves. The data indicated that the multilayer biofilm formation of yeast clusters is expected to increase as a function of the anode current. At near maximum current outputs, the biofilm thickness is anticipated to be the limiting factor in oxygen diffusion to the entire biomass at high glucose concentrations [Glu]. This observation suggested that the long-term operation would decrease the current, as oxygen availability limits the lower layered yeast cells. The lower feedstock ([Glu] = 10−75 mM) in the anode compartment was pseudoproportional to the current density, suggesting the biofilm thickness was not limiting at these concentrations. The electron transport in the biofilm was mainly in the form of a mediated mechanism instead of direct transfer.

Using synergistic factor (α) analysis, the individual contributions of GYMC, YMC+MB, and GYMC+MB MFC configured devices were estimated. The factors indicate that more than 90% of electron transport was mediated and less than 10% was direct through contact with the electrode surface or from glucose directly to the electrode surface. After the MB mediation from complex II/III, the increase in current confirms that the biofilm is far from the electrode surface. The observation also confirms that the yeast cells are metabolically active and involved in electron transfer from microbes to the anodic electrode.

CONCLUSION

A novel proton exchange membrane (PTS) was fabricated using poly(vinyl alcohol) as the matrix, cross-linked by tetraethoxysilane and sulfosuccinic acid. These PTS membranes have a greater solution and similar dry conductance to Nafion. Different formulations with the required water uptake, film conductance, and heat tolerance were generated to offer superior protonic membrane performance in a fully assembled MFC power system. The trinary PTS toolbox allowed by fine-tuning the polymer properties through adjustment of pore volume (more PVA) to conductance (more SSA) to ease of film generation (more TOES), which cross-linked the hydroxyl to silanol to acid groups. It was also found that post functionalization for the membrane through the sodium ion exchange for 20 h enabled the film conductance to be retained with a much lower mass incorporation of SSA. The power and current were higher using PTS as a solid electrolyte at the device level than in Nafion (110%). The microbe *Saccharomyces cerevisiae* was used as a biocatalyst to construct the MFC devices. The variables that yielded the greatest power densities over the unsupported biocatalyst were MB mediation,

https://doi.org/10.1021/acsami.1c20445
ACS Appl. Mater. Interfaces XXXX, XXX, XXX−XXX

RL exposure of 2.88 J cm^{-2}, and GQD anchoring at the anode. A comparison of known literature studies and our data for MB and RL provided a mechanism to explain the increase in power output. Methylene blue in its reduced form (MBH_2) mediates electron transport to cytochrome c directly and is oxidized back to MB. When RL is used, it can also stimulate cytochrome c oxidase and promote electron flux. The increase in current densities after RL exposure could also be explained by the increased yeast oxygen capacity, whereby yeast can metabolize glucose more efficiently. Both increased efficiency in oxygen utilization and a shorter path for electron flow yield higher device power. The in-depth studies show that a power output of up to 300% increase can be achieved by carefully adjusting device configuration to promote electron transfer. Our results suggest that microbial fuel cells showed great promise as a platform for sustainable energy generation with lower cost and emissions than traditional energy production.

MATERIALS AND METHODS

Membrane Synthesis and Characterization. All reagents and chemicals were obtained from VWR International (Houston, TX) and used without further treatment. Distilled water was from our in-house purification systems, and all components for device fabrication were purchased from the FuelCellStore (College Station, TX). The membranes were fabricated by a sol−gel method under homogeneous catalysis. The reaction temperature was controlled at 90 °C for a 2 h duration. Various amounts of SSA and TEOS were added into the PVA solution to tune the porosity, water uptake, and ionic conductivity. The Fourier transform infrared (FT-IR) spectra of the PTS membranes were measured by an IR Prestige-21 Instrument in the range of 2000−700 cm^{-1} and ultraviolet−visible spectroscopy (Evolution 300). A multiparameter meter was used to determine solution pH/conductivity/ORP (VWR Symphony) and dry conductance using either a two-probe (WE/RE) or a four-probe (WE/RE/CE/SE) method.

Microbial Fuel Cell Construction and Evaluation. Dried yeast was dissolved in phosphate-buffered saline (PBS, pH 7.2, 0.1 M) and formulated into a paste with different amounts of carboxymethylcellulose. Asymmetrical MFC devices were assembled using biota-anchored films as the anode catalysts and C−Pt as the cathode catalysts. The MFCs operated in either aerobic or anaerobic mode. To the anode compartment was added glucose (10 mM to 1 M, 15 mL) as feedstock and either PBS (15 mL) or methylene blue (1 ppm, 15 mL in PBS) as the electron mediator. To the cathode compartment was added either PBS (15 mL) or KFC (2 ppm, 15 mL in PBS) as electron acceptor. The membrane electrode assembly (MEA) was constructed with the stainless-steel current collector followed by the gas diffusion layer (GDL, Avcarb, or CeTech). The GDL was coated with yeast-methylcellulose (YMC) as the anode. The PTS member (2.54 cm^2 area scaled to $100/\pi$. This allows conversion to m^2 by ×10. The membrane thickness was 125 μm) with or without Na^+ exchange was used as the solid electrolyte. The MEA was completed with a second GDL and current collector as the cathode. The MEA was connected to the glucose/MB and PBS/KFC reservoirs to construct the MFC device. The device was conditioned for 10 min, and then appropriate current, voltage, and power were measured using an electrochemical power box. The red light with a wavelength of 635 ± 5 nm was applied to the different anodic materials with yeast for varying durations (15−240 min). The output was 5 W, and the exposure area was 80 ± 2 cm^2 with a vertical distance between the yeast layer and the lamp surface of 15 ± 1 cm. The radiant exposure of 2.88 J cm^{-2} corresponded to an illumination time of 60 min.

Electrochemical Performance of MFC Devices. The MFC devices were evaluated using Gamry ref 600 potentiostat (±0.2% accuracy on potential and current readings). Echem Analyst software was used to analyze the collected data. The MFC devices' open circuit potential (OCP) was measured before reaching stability. The electrochemical impedance spectroscopy (EIS) measurements were carried out at OCP over the frequencies from 0.1 Hz to 1 MHz. The 10 mV amplitude sinusoidal voltage was applied as a disturbance signal. The polarization curves were collected at a potential range from 1 V to −1 V versus OCP with a scan rate of 100 mV s^{-1}. All measurements were performed at ambient conditions. A preprogrammed sequence measured the OCP and then the EIS, followed by a 1 h reset period before repeating the measurements to allow device restabilization.

ASSOCIATED CONTENT

Supporting Information

The Supporting Information is available free of charge at https://pubs.acs.org/doi/10.1021/acsami.1c20445.

Video S1, cross-linking between PVA and TOES shown to demonstrate 360° rotation (AVI)

Video S2, a second complex III−IV rotation in yeast shown to better understand electron transport mechanisms (AVI)

AUTHOR INFORMATION

Corresponding Authors

Sajid Bashir − *Department of Chemistry, Texas A&M University-Kingsville, Kingsville, Texas 78363-8202, United States*; orcid.org/0000-0001-5356-8853; Email: br9@tamuk.edu

Shawn P. Mulvaney − *Chemistry Division, U.S. Naval Research Laboratory, Washington, DC 20375-5342, United States*; Email: shawn.mulvaney@nrl.navy.mil

Authors

William Houf − *Department of Chemistry, Texas A&M University-Kingsville, Kingsville, Texas 78363-8202, United States*

Jingbo L. Liu − *Department of Chemistry, Texas A&M University-Kingsville, Kingsville, Texas 78363-8202, United States; Texas A&M Energy Institute, College Station, Texas 77843-3372, United States*

Complete contact information is available at: https://pubs.acs.org/10.1021/acsami.1c20445

Author Contributions

S.B. and S.P.M. conceived this project and administered the funds and research progress. W.F. was trained to produce PTS membranes and characterize their structures. J.L.L. prepared different formulations of PTS, synthesized graphene, and assembled the MFC devices. S.B. and J.L.L. completed the device evaluation and data analyses. The manuscript was written through the contributions of all authors. All authors have approved the final version of the manuscript.

Funding

Texas A&M Energy Institute; the Robert Welch Foundation (Departmental Grant, AC-0006); Office of Naval Research, Summer Faculty Research Program.

Notes

The authors declare no competing financial interest.

ACKNOWLEDGMENTS

This work is supported by the Texas A&M Energy Institute and the Robert Welch Foundation (Departmental Grant, AC-0006). Office of Naval Research, Summer Faculty Research Program. The technical supports from Texas A&M Univer-

sity−Kingsville and Texas A&M Energy Institute are also duly acknowledged.

■ ABBREVIATIONS

MFCs, microbial fuel cells; RL, red light; GDQ, graphene quantum dots

■ REFERENCES

(1) Kim, B. H.; Chang, I. S.; Gadd, G. M. Challenges in microbial fuel cell development and operation. *Appl. Microbiol. Biotechnol.* **2007**, *76*, 485−494.
(2) Kumar, P.; Saroj, D. P. Water-energy-pollution nexus for growing cities. *Urban Clim.* **2014**, *10*, 846−853.
(3) Madiraju, K. S.; Lyew, D.; Kok, R.; Raghavan, V. Carbon-neutral electricity production by Synechocystis sp. PCC6803 in a microbial fuel cell. *Bioresour. Technol.* **2012**, *110*, 214−218.
(4) Ieropoulos, I. A.; Greenman, J.; Melhuish, C.; Hart, J. Comparative study of three types of microbial fuel cells. *Enzyme Microb. Technol.* **2005**, *37* (2), 238−245.
(5) Rahimnejad, M.; Adhami, A.; Darvari, S.; Zirepour, A.; Oh, S. E. The microbial fuel cell as new technology for bioelectricity generation: A review. *Alexandria Eng. J.* **2015**, *54* (3), 745−756.
(6) Gil, G. C.; Chang, I. S.; Kim, B. H.; Kim, M.; Jang, J. K.; Park, H. S.; Kim, H. J. Operational parameters affecting the performance of a mediator-less microbial fuel cell. *Biosens. Bioelectron.* **2003**, *18* (4), 327−334.
(7) Rapoport, B. I.; Kedzierski, J. T.; Sarpeshkar, R. A glucose fuel cell for implantable brain-machine interfaces. *PLoS One* **2012**, *7* (6), e38436.
(8) Zhang, X. C.; Halme, A. Modeling of a microbial fuel cell process. *Biotechnol. Lett.* **1995**, *17* (8), 809−814.
(9) Yuan, Y.; Yuan, T.; Wang, D.; Tang, J.; Zhou, S. Sewage sludge biochar as an efficient catalyst for oxygen reduction reaction in a microbial fuel cell. *Bioresour. Technol.* **2013**, *144*, 115−120.
(10) Davis, J. B.; Yarbrough, H. F. Preliminary experiments on a microbial fuel cell. *Science* **1962**, *137* (3530), 615−616.
(11) Nimje, V. R.; Chen, C.-Y.; Chen, C.-C.; Jean, J.-S.; Reddy, A. S.; Fan, C.-W.; Pan, K.-Y.; Liu, H.-T.; Chen, J.-L. Stable and high energy generation by a strain of *Bacillus subtilis* in a microbial fuel cell. *J. Power Sources* **2009**, *190* (2), 258−263.
(12) Cappadonia, M.; Erning, J. W.; Niaki, S. M. S.; Stimming, U. Conductance of Nafion 117 membranes as a function of temperature and water content. *Solid State Ionics* **1995**, *77*, 65−69.
(13) Kallo, J.; Lehnert, W.; von Helmolt, R. Conductance, and methanol crossover investigation of Nafion membranes in a vapor fed DMFC. *J. Electrochem. Soc.* **2003**, *150* (6), A765.
(14) Faghri, A.; Guo, Z. Challenges and opportunities of thermal management issues related to fuel cell technology and modeling. *Int. J. Heat Mass Transfer* **2005**, *48* (19−20), 3891−3920.
(15) Wakizoe, M.; Velev, O. A.; Srinivasan, S. Analysis of proton exchange membrane fuel cell performance with alternate membranes. *Electrochim. Acta* **1995**, *40* (3), 335−344.
(16) MARTINELLI, A; MATIC, A; JACOBSSON, P; BORJESSON, L; NAVARRA, M; FERNICOLA, A; PANERO, S; SCROSATI, B Structural analysis of PVA-based proton conducting membranes. *Solid State Ion.* **2006**, *177* (26−32), 2431−2435.
(17) Lee, J. S.; Choi, K. H.; Ghim, H. D.; Kim, S. S.; Chun, D. H.; Kim, H. Y.; Lyoo, W. S. Role of molecular weight of atactic poly (vinyl alcohol) (PVA) in the structure and properties of PVA nano fabric prepared by electrospinning. *J. Appl. Polym. Sci.* **2004**, *93* (4), 1638−1646.
(18) Baker, M. I.; Walsh, S. P.; Schwartz, Z.; Boyan, B. D. A review of polyvinyl alcohol and its uses in cartilage and orthopedic applications. *J. Biomed. Mater. Res. B: Appl. Biomater.* **2012**, *100* (5), 1451−1457.
(19) Zhang, R.; Xu, X.; Cao, B.; Li, P. Fabrication of high-performance PVA/PAN composite pervaporation membranes cross-linked by PMDA for wastewater desalination. *Pet. Sci.* **2018**, *15* (1), 146−156.
(20) Lim, M.; Kwon, H.; Kim, D.; Seo, J.; Han, H.; Khan, S. B. Highly enhanced water-resistant and oxygen barrier properties of crosslinked poly (vinyl alcohol) hybrid films for packaging applications. *Prog. Org. Coat.* **2015**, *85*, 68−75.
(21) Yu, H.; Cao, Y.; Fang, Q.; Liu, Z. Effects of treatment temperature on properties of starch-based adhesives. *BioResources* **2015**, *10* (2), 3520−3530.
(22) Mujtaba, M.; Morsi, R. E.; Kerch, G.; Elsabee, M. Z.; Kaya, M.; Labidi, J.; Khawar, K. M. Current advancements in chitosan-based film production for food technology; A review. *Int. J. Biol. Macromol.* **2019**, *121*, 889−904.
(23) Li, H.; Zhang, W.; Xu, W.; Zhang, X. Hydrogen bonding governs the elastic properties of poly (vinyl alcohol) in water: single-molecule force spectroscopic studies of PVA by AFM. *Macromolecules* **2000**, *33* (2), 465−469.
(24) Daemi, H.; Mashayekhi, M.; Pezeshki Modaress, M. Facile fabrication of sulfated alginate electrospun nanofibers. *Carbohydr. Polym.* **2018**, *198*, 481−485.
(25) González-Guisasola, C.; Ribes-Greus, A. Dielectric relaxations and conductivity of crosslinked PVA/SSA/GO composite membranes for fuel cells. *Polym. Test.* **2018**, *67*, 55−67.
(26) Pirzada, T.; Arvidson, S. A.; Saquing, C. D.; Shah, S. S.; Khan, S. A. Hybrid silica-PVA nanofibers via sol-gel electrospinning. *Langmuir* **2012**, *28* (13), 5834−5844.
(27) Mansur, H. S.; Oréfice, R. L.; Mansur, A. A. Characterization of poly (vinyl alcohol)/poly (ethylene glycol) hydrogels and PVA-derived hybrids by small-angle X-ray scattering and FTIR spectroscopy. *Polymer* **2004**, *45* (21), 7193−7202.
(28) Bashir, S.; Mulvaney, S. P.; Houf, W.; Villanueva, L.; Wang, Z.; Buck, G.; Liu, J. L. Microbial Fuel Cells: Design and Evaluation of Catalysts and Device. In *Advances in Sustainable Energy*; Springer, 2021; pp 681−764. .
(29) Canto-Canche, B.; Carreon-Anguiano, K. G.; Barahona-Cortes, R.; Canseco-Perez, M. A.; Chi-Manzanero, B.; Mena-Espino, X.; Tzec-Sima, M.; Islas-Flores, I.; Espana-Gamboa, E. I.; Barahona-Perez, L. F.; et al. Use of Agroindustrial Biomass for Biofuel and Enzyme Discovery and Production. *Agricultural, Forestry and Bioindustry Biotechnology and Biodiscovery* **2020**, 271−318.
(30) Rahimnejad, M.; Najafpour, G. D.; Ghoreyshi, A. A.; Talebnia, F.; Premier, G. C.; Bakeri, G.; Kim, J. R.; Oh, S.-E. Thionine increases electricity generation from a microbial fuel cell using *Saccharomyces cerevisiae* and exoelectrogenic mixed culture. *J. Microbiol* **2012**, *50* (4), 575−580.
(31) Rossi, R.; Fedrigucci, A.; Setti, L. Characterization of electron mediated microbial fuel cell by *Saccharomyces cerevisiae*. *Chem. Eng. Trans* **2015**, *43*, 337−342.
(32) Zhong, L.; Song, Y.; Zhou, S. The Effectiveness of Nafion-Coated Stainless-Steel Surfaces for Inhibiting *Bacillus Subtilis* Biofilm Formation. *Appl. Sci.* **2020**, *10* (14), 5001.
(33) Arbianti, R.; Hermansyah, H.; Utami, T. S.; Zahara, N. C.; Trisnawati, I.; Kristin, E. The usage of *Saccharomyces cerevisiae* in microbial fuel cell system for electrical energy production. *J. Chem. Chem. Eng.* **2012**, *6* (9), 814.
(34) Gunawardena, A.; Fernando, S.; To, F. Performance of a yeast-mediated biological fuel cell. *Int. J. Mol. Sci.* **2008**, *9* (10), 1893−1907.
(35) Lin, T.; Bai, X.; Hu, Y.; Li, B.; Yuan, Y.-J.; Song, H.; Yang, Y.; Wang, J. Synthetic *Saccharomyces cerevisiae-Shewanella oneidensis* consortium enables glucose-fed high-performance microbial fuel cells. *AIChE J.* **2017**, *63* (6), 1830−1838.
(36) Han, J.; Lei, T.; Wu, Q. High-water-content mouldable polyvinyl alcohol-borax hydrogels reinforced by well-dispersed cellulose nanoparticles: Dynamic rheological properties and hydrogel formation mechanism. *Carbohydr. Polym.* **2014**, *102*, 306−316.
(37) Karim, M. R.; Islam, M. Thermal behavior with a mechanical property of fluorinated silane functionalized superhydrophobic pullulan/poly (vinyl alcohol) blends by electrospinning method. *J. Nanomater.* **2011**, *2011*, 979458.

https://doi.org/10.1021/acsami.1c20445
ACS Appl. Mater. Interfaces XXXX, XXX, XXX−XXX

(38) Kim, D. S.; Park, H. B.; Rhim, J. W.; Lee, Y. M. Proton conductivity and methanol transport behavior of crosslinked PVA/PAA/silica hybrid membranes. *Solid State Ionics* **2005**, *176* (1−2), 117−126.
(39) Rhim, J. W.; Yeom, C. K.; Kim, S. W. Modification of poly (vinyl alcohol) membranes using sulfur-succinic acid and its application to pervaporation separation of water-alcohol mixtures. *J. Appl. Polym. Sci.* **1998**, *68* (11), 1717−1723.
(40) Hong, X.; Xu, Y.; Zou, L.; Li, Y. V.; He, J.; Zhao, J. The effect of degree of polymerization on the structure and properties of polyvinyl alcohol fibers with high strength and high modulus. *J. Appl. Polym. Sci.* **2021**, *138* (10), 49971.
(41) Zhou, J.; Lin, S.; Zeng, H.; Liu, J.; Li, B.; Xu, Y.; Zhao, X.; Chen, G. Dynamic intermolecular interactions through hydrogen bonding of water promote heat conduction in hydrogels. *Mater. Horiz.* **2020**, *7* (11), 2936−2943.
(42) Tsai, C. E.; Lin, C. W.; Hwang, B. J. A novel crosslinking strategy for preparing poly (vinyl alcohol)-based proton-conducting membranes with high sulfonation. *J. Power Sources* **2010**, *195* (8), 2166−2173.
(43) Vani, R.; Ramaprabhu, S.; Haridoss, P. Mechanically stable and economically viable polyvinyl alcohol-based membranes with sulfonated carbon nanotubes for proton exchange membrane fuel cells. *Sustain. Energy Fuels.* **2020**, *4* (3), 1372−1382.
(44) Maiti, J.; Kakati, N.; Lee, S. H.; Jee, S. H.; Yoon, Y. S. PVA nanocomposite membrane for DMFC application. *Solid State Ionics* **2011**, *201* (1), 21−26.
(45) Li, L.; Xu, X.; Liu, L.; Song, P.; Cao, Q.; Xu, Z.; Fang, Z.; Wang, H. Water governs the mechanical properties of poly (vinyl alcohol). *Polymer.* **2021**, *213*, 123330.
(46) Gil-Castell, O.; Teruel-Juanes, R.; Arenga, F.; Salaberria, A.M.; Baschetti, M.G.; Labidi, J.; Badia, J.D.; Ribes-Greus, A. Crosslinked chitosan/poly (vinyl alcohol)-based polyelectrolytes for proton exchange membranes. *React. Funct. Polym.* **2019**, *142*, 213−222.
(47) Kaneshiro, H.; Takano, K.; Takada, Y.; Wakisaka, T.; Tachibana, T.; Azuma, M. A milliliter-scale yeast-based fuel cell with high performance. *Biochem. Eng. J.* **2014**, *83*, 90−96.
(48) Morin, P. E.; Freire, E. Direct calorimetric analysis of the enzymic activity of yeast cytochrome c oxidase. *Biochemistry* **1991**, *30* (34), 8494−8500.
(49) Christwardana, M.; Frattini, D.; Accardo, G.; Yoon, S. P.; Kwon, Y. Optimization of glucose concentration and glucose/yeast ratio in yeast microbial fuel cells using response surface methodology approach. *J. Power Sources* **2018**, *402*, 402−412.
(50) Sayed, E. T.; Alawadhi, H.; Olabi, A. G.; Jamal, A.; Almah-di, M. S.; Khalid, J.; Abdelkareem, M. A. Electrophoretic deposition of GQDs oxide on carbon brush as bioanode for microbial fuel cell operated with real wastewater. *Int. J. Hydrogen Energy* **2021**, *46* (8), 5975−5983.
(51) Urban, P. F.; Klingenberg, M. On the redox potentials of ubiquinone and cytochrome b in the respiratory chain. *Eur. J. Biochem.* **1969**, *9* (4), 519−525.
(52) Otterstedt, K.; Larsson, C.; Bill, R. M.; Ståhlberg, A.; Boles, E.; Hohmann, S.; Gustafsson, L. Switching the mode of metabolism in the yeast *Saccharomyces cerevisiae*. *EMBO Rep.* **2004**, *5* (5), 532−537.
(53) Wu, M.; Repetto, B.; Glerum, D. M.; Tzagoloff, A. Cloning and characterization of FAD1, the structural gene for flavin adenine dinucleotide synthetase of *Saccharomyces cerevisiae*. *Mol. Cell. Biol.* **1995**, *15* (1), 264−271.
(54) Kaneshiro, H.; Takano, K.; Takada, Y.; Wakisaka, T.; Tachibana, T.; Azuma, M. A milliliter-scale yeast-based fuel cell with high performance. *Biochem. Eng. J.* **2014**, *83*, 90−96.
(55) Santos-Ocaña, C.; Villalba, J. M.; Córdoba, F.; Padilla, S.; Crane, F. L.; Clarke, C. F.; Navas, P. Genetic evidence for coenzyme Q requirement in plasma membrane electron transport. *J. Bioenerg. Biomembr.* **1998**, *30* (5), 465−475.
(56) Kulys, J.; Wang, L.; Razumas, V. Sensitive yeast bioelectrode to L-lactate. *Electroanalysis* **1992**, *4* (5), 527−532.
(57) Marsili, E.; Rollefson, J. B.; Baron, D. B.; Hozalski, R. M.; Bond, D. R. Microbial biofilm voltammetry: direct electrochemical characterization of catalytic electrode-attached biofilms. *Appl. Environ. Microbiol.* **2008**, *74* (23), 7329−7337.
(58) Schröder, U. Anodic electron transfer mechanisms in microbial fuel cells and their energy efficiency. *Phys. Chem. Chem. Phys.* **2007**, *9* (21), 2619−2629.
(59) Babanova, S.; Hubenova, Y.; Mitov, M. Influence of artificial mediators on yeast-based fuel cell performance. *J. Biosci. Bioeng.* **2011**, *112* (4), 379−387.
(60) Lee, K. K.; Imaizumi, N.; Chamberland, S. R.; Alder, N. N.; Boelsterli, U. A. Targeting mitochondria with methylene blue protects mice against acetaminophen-induced liver injury. *Hepatology* **2015**, *61* (1), 326−336.
(61) Schwall, C. T.; Greenwood, V. L.; Alder, N. N. The stability and activity of respiratory Com-plex II are cardiolipin-dependent. *Biochim. Biophys. Acta, Bioenerg.* **2012**, *1817* (9), 1588−1596.
(62) Lee, K. K.; Boelsterli, U. A. Bypassing the compromised mitochondrial electron transport with methylene blue alleviates efavirenz/isoniazid-induced oxidant stress and mitochondria-mediated cell death in mouse hepatocytes. *Redox Biol.* **2014**, *2*, 599−609.
(63) Christwardana, M.; Frattini, D.; Accardo, G.; Yoon, S. P.; Kwon, Y. Effects of methylene blue and methyl red mediators on the performance of yeast-based microbial fuel cells adopting polyethyleneimine coated carbon felt as an anode. *J. Power Sources* **2018**, *396*, 1−11.
(64) Prasad, D.; Arun, S.; Murugesan, M.; Padmanaban, S.; Satyanarayanan, R. S.; Berchmans, S.; Yegnaraman, V. Direct electron transfer with yeast cells and construction of a mediatorless microbial fuel cell. *Biosens. Bioelectron.* **2007**, *22* (11), 2604−2610.
(65) Stuart, R. A.; Cruciat, C. M.; Brunner, S.; Baumann, F.; Neupert, W. The Cytochrome bc^1 and Cytochrome Oxidase Complexes Associate to Form a Single Supracomplex in Yeast Mitochondria. *J. Biol. Chem.* **2000**, *275* (24), 18093−18098.
(66) Lin, A.-L.; Poteet, E.; Du, F.; Gourav, R. C.; Liu, R.; Wen, Y.; Bresnen, A.; Huang, S.; Fox, P. T.; Yang, S.-H.; Duong, T. Q. Methylene blue is a cerebral metabolic and hemodynamic enhancer. *Plos one.* **2012**, *7*, e46585.
(67) Wen, Y.; Li, W.; Poteet, E. C.; Xie, L.; Tan, C.; Yan, L.-J.; Ju, X.; Liu, R.; Qian, H.; Marvin, M. A.; et al. Alternative mitochondrial electron transfer as a novel strategy for neuroprotection. *J. Biol. Chem.* **2011**, *286* (18), 16504−16515 (2011).

https://doi.org/10.1021/acsami.1c20445
ACS Appl. Mater. Interfaces XXXX, XXX, XXX−XXX